Hydrology and
Earth System
Sciences
Discussions

Open Access

Closing the water balance with cosmic-ray soil moisture measurements and assessing their spatial variability within two semiarid watersheds

A. P. Schreiner-McGraw[1], E. R. Vivoni[1,2], G. Mascaro[3], and T. E. Franz[4]

[1]School of Earth and Space Exploration, Arizona State University, Tempe, AZ, 85287, USA
[2]School of Sustainable Engineering and the Built Environment, Arizona State University, Tempe, AZ, 85287, USA
[3]Julie Ann Wrigley Global Institute of Sustainability, Arizona State University, Tempe, AZ, 85287, USA
[4]School of Natural Resources, University of Nebraska-Lincoln, Lincoln, NE, 68583, USA

Correspondence to: E. R. Vivoni (vivoni@asu.edu)

Discussion Paper | Discussion Paper | Discussion Paper | Discussion Paper |

HESSD

12, 5343–5388, 2015

Water balance with cosmic-ray soil moisture data

A. P. Schreiner-McGraw et al.

Title Page

Abstract | Introduction

Conclusions | References

Tables | Figures

◄◄ | ►►

◄ | ►

Back | Close

Full Screen / Esc

Printer-friendly Version

Interactive Discussion

Water balance with cosmic-ray soil moisture data

A. P. Schreiner-McGraw et al.

Abstract

Soil moisture dynamics reflect the complex interactions of meteorological conditions with soil, vegetation and terrain properties. In this study, intermediate scale soil moisture estimates from the cosmic-ray sensing (CRS) method are evaluated for two semiarid ecosystems in the southwestern United States: a mesquite savanna at the Santa Rita Experimental Range (SRER) and a mixed shrubland at the Jornada Experimental Range (JER). Evaluations of the CRS method are performed for small watersheds instrumented with a distributed sensor network consisting of soil moisture sensor profiles, an eddy covariance tower and runoff flumes used to close the water balance. We found an excellent agreement between the CRS method and the distributed sensor network (RMSE of 0.009 and 0.013 $m^3 m^{-3}$ at SRER and JER) at the hourly time scale over the 19-month study period, primarily due to the inclusion of 5 cm observations of shallow soil moisture. Good agreement was obtained in soil moisture changes estimated from the CRS and watershed water balance methods (RMSE = 0.001 and 0.038 $m^3 m^{-3}$ at SRER and JER), with deviations due to bypassing of the CRS measurement depth during large rainfall events. This limitation, however, was used to show that drier-than-average conditions at SRER promoted plant water uptake from deeper layers, while the wetter-than-average period at JER resulted in leakage towards deeper soils. Using the distributed sensor network, we quantified the spatial variability of soil moisture in the CRS footprint and the relation between evapotranspiration and soil moisture, in both cases finding similar predictive relations at both sites that are applicable to other semiarid ecosystems in the southwestern US. Furthermore, soil moisture spatial variability was related to evapotranspiration in a manner consistent with analytical relations derived using the CRS method, opening up new possibilities for understanding land-atmosphere interactions.

A. P. Schreiner-McGraw et al.

1   Introduction

Soil moisture is a key land surface variable that governs important processes such as the rainfall-runoff transformation, the partitioning of latent and sensible heat fluxes and the spatial distribution of vegetation in semiarid regions (e.g., Entekhabi, 1995; Eltahir, 1998; Vivoni, 2012). Semiarid watersheds with heterogeneous vegetation in the southwestern United States (Gibbens and Beck, 1987; Browning et al., 2014) exhibit variations in soil moisture that challenge our ability to quantify land-atmosphere interactions and their role in hydrological processes (Dugas et al., 1996; Small and Kurc, 2003; Scott et al., 2006; Gutiérrez-Jurado et al., 2013; Pierini et al., 2014). Moreover, accurate measurements of soil moisture over scales relevant to land-atmosphere interactions in watersheds are difficult to obtain. Traditionally, soil moisture is measured continuously at single locations using techniques such as time domain reflectometry and then aggregated in space using a number of methods (Topp et al., 1980; Western et al., 2002; Vivoni et al., 2008b). Soil moisture is also estimated using satellite-based techniques, such as passive microwave sensors, but spatial resolutions are typically coarse and overpass times infrequent (e.g., Kustas et al., 1998; Moran et al., 2000; Narayan and Lakshmi, 2008), as compared to the spatiotemporal variability of soil moisture in semi-arid watersheds.

One approach to address the scale gap in soil moisture estimation is through the use of cosmic-ray sensing (CRS) measurements (Zreda et al., 2008, 2012) that provide soil moisture with a measurement footprint of several hectares (Desilets et al., 2010). Developments of the CRS method have focused on understanding the processes affecting the measurement technique, for example, the effects of vegetation growth (Franz et al., 2013a; Coopersmith et al., 2014), atmospheric water vapor (Rosolem et al., 2013), soil wetting and drying (Franz et al., 2012a) and horizontal heterogeneity (Franz et al., 2013b). To date, the validation of the CRS method has been performed using single site measurements, aggregations of different measurement locations and particle transport models (Desilets et al., 2010; Franz et al., 2013b; Zhu et al., 2015). At the watershed

scale, however, the CRS method can also be validated based upon the application of the water balance equation, as performed for the eddy covariance (EC) technique often used to measure surface turbulent fluxes (Scott, 2010; Templeton et al., 2014). In small watersheds of comparable size to the CRS measurement footprint, the water balance can be expressed as:

$$z_m \frac{\Delta \theta}{\Delta t} = P - \mathrm{ET} - Q - L, \tag{1}$$

where θ is volumetric soil moisture, P is precipitation, ET is evapotranspiration, Q is streamflow, and L is leakage, with all of the terms expressed as spatially-averaged quantities and valid over the effective soil measurement depth (z_m). Closing the water balance, or the estimation of each term of Eq. (1), would be a novel way for comparing the CRS method to independent observations valid at a commensurate spatial and temporal scale. Nevertheless, the application of Eq. (1) can be fraught with issues related to measurement limitations and representativeness or when spatially-averaged quantities are difficult to obtain in heterogeneous watersheds.

Soil moisture measurements at the intermediate scales provided by the CRS method do not capture the spatial variability within the measurement footprint (Zreda et al., 2008). As a result, distributed sensor networks consisting of different locations in a watershed are essential for establishing how the spatially-averaged properties are obtained (e.g., Franz et al., 2012b). Capturing the soil moisture spatial variability within a measurement footprint is also important for improving the representation of land-atmosphere interactions and hydrologic processes in models (Famiglietti and Wood, 1994; Bindlish et al., 2009; Mascaro and Vivoni, 2012). Based on prior studies using distributed sensor networks, the spatial variability of soil moisture is expected to increase with wetter spatially-averaged conditions in the range of values observed in semiarid areas (Famiglietti et al., 1999; Lawrence and Hornberger, 2007; Fernández and Ceballos, 2003; Vivoni et al., 2008b; Mascaro et al., 2011), as heterogeneities related to vegetation, terrain position and soil properties progressively lead to larger

spatial differences within a watershed. Soil moisture variability also impacts land-atmosphere interactions by influencing soil evaporation and plant transpiration. ET measurements using the EC technique also have an intermediate spatial scale depending on wind speed and direction, atmospheric stability, and instrument and surface roughness heights (e.g., Hsieh et al., 2000; Kormann and Meixner, 2001; Falge et al., 2002). Thus, the use of the CRS method and a distributed sensor network could yield valuable information on how soil moisture and its spatial variability affect evapotranspiration losses. Furthermore, the relation between ET and soil moisture is an important parameterization in models (e.g., Laio et al., 2001; Rodríguez-Iturbe and Porporato, 2004; Vivoni et al., 2008a), which could be improved at intermediate spatial scales through a link between the spatial variability of soil moisture and the aggregated evapotranspiration flux.

In this contribution, we study the soil moisture dynamics of two semiarid watersheds in Arizona and New Mexico through a comparison of the CRS method with a distributed sensor network and estimates from closing the water balance at each site. To our knowledge, this is the first study where CRS measurements are validated to two independent methods at the small watershed scale. The two watersheds represent the heterogeneous vegetation and soil conditions observed in the Sonoran and Chihuahuan Deserts of the southwestern US (Templeton et al., 2014; Pierini et al., 2014). Given the simultaneous observations during the study period (March 2013 to September 2014, 19 months) at both sites, we compare the variations in vadose zone processes (infiltration, plant water uptake, leakage) that differentially occur at each site in response to varying precipitation. Combining these various measurement techniques also affords the capacity to construct and compare relationships between the spatially-averaged CRS estimates and the spatial variability of soil moisture in the measurement footprint as well as with the spatially-averaged ET obtained from the EC method. Finally, by complementing the CRS and EC observations with the distributed sensor network, we propose and test an analytical relation that describes how evapotranspiration varies with the spatial variability of soil moisture.

2 Methods

2.1 Study sites and their general characteristics

The two study sites are long-term experimental watersheds in semiarid ecosystems of the southwestern United States. Watershed monitoring began in 1975 at the Santa Rita Experimental Range (SRER), located 45 km south of Tucson, Arizona, in the Sonoran Desert (Fig. 1), as described by Polyakov et al. (2010) and Scott (2010). Precipitation at the site varies considerably during the year, with 54 % of the long-term mean amount (364 mm/yr) occurring during the summer months of July to September due to the North American monsoon (Vivoni et al., 2008a; Pierini et al., 2014). Soils at the SRER site are a coarse-textured sandy loam (Anderson, 2013) derived from Holocene-aged alluvium from the nearby Santa Rita Mountains. The savanna ecosystem at the site consists of the velvet mesquite tree (*Prosopis velutina* Woot.), interspersed with grasses (*Eragrostis lehmanniana*,*Bouteloua rothrockii*,*Muhlenbergia porteri* and *Aristida glabrata*) and various cacti species (*Opuntia spinosior*,*Opuntia engelmannii* and *Ferocactus wislizeni*). Similarly, watershed monitoring began in 1977 at the Jornada Experimental Range (JER), located 30 km north of Las Cruces, New Mexico, in the Chihuahuan Desert (Fig. 1), as described by Turnbull et al. (2013). Mean annual precipitation at the JER is considerably lower than SRER (251 mm/yr), with a similar proportion (53 %) occurring during the summer monsoon (Templeton et al., 2014). Soils at the JER site are primarily sandy loam with high gravel contents (Anderson, 2013) transported from the San Andreas Mountains. The mixed shrubland ecosystem at the site consists of creosote bush (*Larrea tridentata*), honey mesquite (*Prosopis glandulosa* Torr.), several grass species (*Muhlenbergia porteri*, *Pleuraphis mutica* and *Sporobolus cryptandrus*), and other shrubs (*Parthenium incanum*, *Flourensia cernua* and *Gutierrezia sarothrae*). Figure 2 presents a vegetation classification at each site grouped into major categories: (1) SRER has velvet mesquite (labeled mesquite), grasses, cacti (*Opuntia engelmannii* or prickly pear) and bare soil, while (2) JER has honey mesquite (labeled mesquite), creosote bush, other shrubs, grasses

and bare soil. Table 1 presents the vegetation and geomorphological properties for the site watersheds obtained from 1-m digital elevation models (DEMs) and 1 m vegetation maps (Fig. 2). Pierini et al. (2014) and Templeton et al. (2014) describe the image acquisition and processing methods employed to derive these products at SRER and JER, respectively.

2.2 Distributed sensor networks at the small watershed scale

Long-term watershed monitoring at the SRER and JER sites consisted of rainfall and runoff observations at Watersheds 7 and 8 (SRER, 1.25 ha) and the Tromble Weir (JER, 4.67 ha). Pierini et al. (2014) and Templeton et al. (2014) describe recent monitoring efforts using a network of rainfall, runoff, soil moisture and temperature observations as well as radiation and energy balance measurements at EC towers, commencing in 2011 and 2010 at SRER and JER. This brief description of the distributed sensor networks is focused on the spatially-averaged measurements used for comparisons to the CRS method. Precipitation (P) was measured using multiple tipping-bucket rain gauges (TE525MM, Texas Electronics) to construct a 30 min resolution spatial average based on Thiessen polygons within the watershed boundaries. At the watershed outlets, streamflow (Q) was estimated at Santa Rita supercritical runoff flumes (Smith et al., 1981) using a pressure transducer (CS450, Campbell Scientific Inc.) and an in situ linear calibration to obtain 30 min resolution observations. Evapotranspiration (ET) was obtained at 30 min resolution using the EC technique that employs a three-dimensional sonic anemometer (CSAT3, Campbell Scientific Inc.) and an open path infrared gas analyzer (LI-7500, LI-COR Inc.) installed at 7 min height on each tower. Flux corrections for the EC measurements followed Scott et al. (2004) and were verified using an energy balance closure approach reported in Table 2 for the study period. Energy balance closure at both sites is within the reported values across a range of other locations where the ratio of $\Sigma(\lambda E + H) / \Sigma(R_n - G)$ has an average value of 0.8 (Wilson et al., 2002; Scott, 2010). To summarize these observations, Fig. 3 shows the spatially-averaged P, Q and ET (mm h^{-1}), each aggregated to hourly resolution, at each study site during 1 March

2013 to 30 September 2014, along with seasonal precipitation amounts. While the results compare favorably to previous measurements (Turnbull et al., 2013; Pierini et al., 2014; Templeton et al., 2014), it should be noted that ET and Q data are assumed to represent the spatially-averaged watershed conditions, despite the small mismatch between the watershed boundaries and EC footprints (Fig. 2) and the summation of Q in the two watersheds at SRER.

Distributed soil moisture measurements were obtained using soil dielectric probes (Hydra Probe, Stevens Water) organized as profiles (sensors placed at 5, 15 and 30 cm depths) in each study site as: (1) at SRER, we installed three transects of 5 profiles each located under different vegetation classes (mesquite, grass, prickly pear and bare soil), and (2) at JER, we established three transects of 5 profiles each installed along different hillslopes (north-, south- and west-facing), as shown in Fig. 1. As described in Campbell (1990), individual sensors measure the impedance of an electric signal through a 40.3 cm^3 soil volume (5.7 cm in length and 3.0 cm in diameter) to determine the volumetric soil moisture (θ) in m^3 m^{-3} and soil temperature in °C as 30 min averaged values. A "loam" calibration equation was used in the conversion to θ (Seyfried et al., 2005) and corrected using relations established through gravimetric soil sampling at each study site (a power law relation at SRER with $R^2 = 0.99$ and a linear relation at JER with $R^2 = 0.97$), following Pierini (2013). Spatial averaging of the sensor profiles within the watersheds aggregated to an hourly resolution was performed using a specific weighting scheme for each site based on the main controls on the soil moisture distribution depending on watershed characteristics: (1) at SRER, we utilized the percentage area of each vegetation class (Table 1) and the associated sensor locations within each type (Pierini et al., 2014), and (2) at JER, we accounted for the aspect and elevation at the sensor locations and used these to extrapolate to other locations with similar characteristics based on the 1-m DEM (Templeton et al., 2014).

Water balance with cosmic-ray soil moisture data

A. P. Schreiner-McGraw et al.

Title Page

Abstract | Introduction

Conclusions | References

Tables | Figures

◄ | ►

◄ | ►

Back | Close

Full Screen / Esc

Printer-friendly Version

Interactive Discussion

2.3 Cosmic-ray soil moisture sensing method

The CRS method relates soil moisture to the density of fast or moderated neutrons (Zreda et al., 2008) measured above the soil surface. A cosmic-ray neutron sensor (CRS-1000/B, Hydroinnova LLC) was installed in each watershed in January 2013 to record neutron counts at hourly intervals. We selected the study period (1 March 2013 to 30 September 2014) to coincide with the availability of data from the distributed sensor networks. While the theory of using neutrons for soil moisture measurements has a long history (e.g., Gardner and Kirkham, 1952), recent developments in the measurement of neutrons generated from cosmic rays has increased the horizontal scale, reduced the need for manual sampling and led to a non-invasive approach. Zreda et al. (2008) and Desilets and Zreda (2013) describe the horizontal scale as having a radius of ~ 300 m at sea level and a vertical aggregation scale ranging from 12 to 76 cm depending on soil wetness. Since the travel speed of fast neutrons is > 10 km s^{-1}, neutron mixing occurs instantaneous in the air above the soil surface (Glasstone and Edlund, 1952), providing a well-mixed region that can be sampled with a single detector.

Using a particle transport model, Desilets et al. (2010) found a theoretical relationship between the neutron count rate at a detector and soil moisture for homogeneous SiO$_2$ sand:

$$\theta(N) = \frac{0.0808}{\left(\frac{N}{N_o}\right) - 0.372} - 0.115, \tag{2}$$

where θ (m^3 m^{-3}) is volumetric soil moisture, N is the neutron count rate (counts h^{-1}) normalized to the atmospheric pressure and solar activity level, and N_o (counts h^{-1}) is the count rate over a dry soil under the same reference conditions. The corrections applied to the neutron count rate are detailed in Desilets and Zreda (2003) and Zreda et al. (2012) and are applied automatically in the COSMOS website (http://cosmos.hwr. arizona.edu/). Additionally, since neutron counts are affected by all sources of hydrogen in the support volume, we apply a correction (C_{WV}) for atmospheric water vapor that

was derived by Rosolem et al. (2013) as:

$$C_{WV} = 1 + 0.0054 \left(\rho_v^o - \rho_v^{ref} \right), \tag{3}$$

where ρ_v^o $(\mathrm{g\,m^{-3}})$ and ρ_v^{ref} $(\mathrm{g\,m^{-3}})$ are absolute water vapors at current and reference conditions. To estimate N_o, we performed a manual soil sampling at 18 locations within the CRS footprint (sampled every 60 degrees at radial distances of 25, 75 and 200 m from the detector) at 6 depths (0–5, 5–10, 10–15, 15–20, 20–25, 25–30 cm) for a total of 108 samples per site. Gravimetric soil moisture measurements were made following oven drying at 105 °C for 48 hrs (Dane and Topp, 2002) and converted to volumetric soil moisture using the soil bulk density. The spatially-averaged soil moisture was related to the average neutron count obtained for the same time period (6-hr average) resulting in $N_o = 3973$ at SRER and $N_o = 4724$ at JER, considered to be in line with the expected amounts given the elevations of both sites (Table 1). We applied a 12 h boxcar filter, which ignored rainfall periods with large increase in θ, to the measured count rates to remove the statistical noise associated with the measurement method (Zreda et al., 2012). We note that additional terms to the calibration accounting for variations in lattice water, soil organic carbon and vegetation have been proposed (Zreda et al., 2012; Bogena et al., 2013; McJannet et al., 2014; Coopersmith et al. 2014). However, given the relatively small amount of biomass ($> 2.5\,\mathrm{kg\,m^{-2}}$ at SRER, Huang et al., 2007; and $> 0.5\,\mathrm{kg\,m^{-2}}$ at JER, Huenneke et al., 2001), low soil organic carbon ($4.2\,\mathrm{mg\,C\,g^{-1}}$ soil at SRER; and $2.7\,\mathrm{mg\,C\,g^{-1}}$ soil at JER, Throop et al., 2011), and low clay percent (5.1 % at SRER; and 4.8 % at JER, Anderson, 2013), and thus low lattice water amounts (Greacen, 1981), we have neglected these small terms in the analysis.

Fig. 2 presents the horizontal aggregation scale of the CRS method in comparison to the watershed boundaries and to the EC footprints obtained for summer 2013 (Anderson, 2013). Since both the CRS and EC footprints have horizontally-decaying contributions, we limited the size of the analysis region to the 50 % contribution or source area. While the CRS horizontal footprint is nearly fixed in time at a 120 m radius at SRER and 125 m radius at JER for the 50 % contribution, the EC footprint varies considerably

(Anderson, 2013), with temporal changes occurring in the amount of overlap with the watersheds and CRS footprints. Nevertheless, the vegetation distributions sampled in the CRS, EC and watershed areas (Fig. 2) are nearly the same (Vivoni et al., 2014), such that CRS and EC measurements are considered representative of the watershed conditions. In contrast to the fixed horizontal scale, the CRS method measures a time-varying vertical scale that depends on the soil water content. Franz et al. (2012b) used a particle transport model to determine that the CRS measurement depth, z^*, varied with soil moisture as:

$$z^*(\theta) = \frac{5.8}{\rho_{bd}\tau + \theta + 0.0829},$$ (4)

where ρ_{bd} is dry bulk density of the soil ($1.535\,\mathrm{g\,cm^{-3}}$ at SRER and $1.300\,\mathrm{g\,cm^{-3}}$ at JER) and τ is the weight fraction of lattice water in the mineral grains and bound water, established at 0.02 g/g at each site given the weathered soils (Franz et al., 2012b). To account for this temporal variation, the distributed sensor profiles representing different soil layers (0–10, 10–20, and 20–40 cm in depth) were weighted based on z^* at each hourly time step according to:

$$wt(z) = a\left(1 - \left(\frac{z}{z^*}\right)^b\right) \text{ for } 0 \le wt \le z^*,$$ (5)

where wt(z) is the weight at depth z, a is a constant defined to integrate the profile to unity ($a = 1/\left(z^* - \left(z^{*b+1}/[z^{*b}(b+1)]\right)\right)$) and b controls the shape of the weighting function. For simplicity, we assumed a value of $b = 1$ leading to a linear relationship (Franz et al., 2012b).

2.4 CRS and distributed sensor network analyses methods

We compared hourly soil moisture observations obtained from the CRS method (θ_{CRS}) to estimates from the distributed sensor network (θ_{SN}) that have been averaged in

space (i.e., based on vegetation type at SRER and elevation/aspect location at JER) and depth-weighted according to the time-varying CRS measurement depth (z^*). We also assessed the CRS method relative to estimates from closing the water balance (1) using spatially-averaged P, Q and ET. For this comparison, the change in soil moisture
5 from the water balance ($\Delta\theta_{WB}$) was compared to $\Delta\theta_{CRS}$, both calculated as differences over the time scale of a rainfall event and its soil moisture response (i.e., the change from pre-storm soil moisture to the peak amount due to a rainfall event). This relative comparison assumes an effective soil measurement depth (z_m) of 40 cm determined as the time-averaged z^* from the CRS method at each site. Since this comparison is
10 performed over a short time interval during the rising limb of the soil moisture response, we tested whether the assumption of no leakage (i.e., $L = 0$) is valid given that there are small losses below z_m to the deep vadose zone. Leakage beyond 40 cm is infrequent at both sites during the summer monsoon, but can occur on a time scale of several days during winter precipitation (e.g., Franz et al., 2012b; Templeton et al., 2014; Pierini et
15 al., 2014). We used several metrics to quantitatively assess the comparisons with the CRS method: Root Mean Square Error (RMSE), Correlation Coefficient (CC), Bias (B) and Standard Error of Estimates (SEE).

We also calculated a soil water balance based on the CRS method to determine the spatially-averaged fluxes into and out from the measurement depth (z^*) as (Franz et
20 al., 2012b):

$$f_{CRS}(t) = \left(\theta_{CRS,t} - \theta_{CRS,t-1}\right) \min(z_t^*, z_{t-1}^*)/\Delta t, \tag{6}$$

where f_{CRS} is the daily flux (mm d^{-1}) and Δt is the time step (1 day). Positive values of f_{CRS} represent infiltration (I) into the measurement depth, while negative values equal outflow (O), occurring either as evapotranspiration or leakage. Based on daily P data,
25 Q can be derived as $P - I$, assuming negligible plant interception, and compared to Q measurements in the watersheds. Using the EC method to obtain daily ET, $L = O -$ ET can be obtained as a measure of exchanges between the CRS measurement depth

and soil below z^*. L is positive when there is leakage to deeper soil layers and negative when deeper water is being drawn to support plant transpiration.

2.5 Soil moisture variability and its link to evapotranspiration

The spatial variability within the CRS footprint was assessed using the distributed sensor network by constructing relations between the spatial standard deviation (σ) and coefficient of variation (CV $= \sigma / <\theta>$) with the mean soil moisture state ($<\theta>$), obtained either from the CRS method (θ_{CRS}) or distributed sensor network (θ_{SN}). Based on the methods proposed by Famiglietti et al. (2008), we fitted the following empirical functions to the observations at each site:

$$\sigma = k_1 \langle\theta\rangle e^{-k_2\langle\theta\rangle} \tag{7}$$

and

$$CV = k_1 e^{-k_2\langle\theta\rangle}, \tag{8}$$

where k_1 and k_2 are regression parameters, and compared these to prior studies in the region (e.g., Vivoni et al., 2008b; Mascaro and Vivoni, 2012; Stillman et al., 2014). Soil moisture at single locations is typically linked to evapotranspiration in hydrologic models (e.g., Chen et al., 1996; Ivanov et al., 2004) and empirical studies (e.g., Small and Kurc, 2003; Vivoni et al., 2008a) using relations such as ET $= f(\theta)$. For example, a commonly used approach is based on a piecewise linear relation between daily ET and θ (Rodríguez-Iturbe and Porporato, 2004):

$$ET(\theta) = \begin{cases} 0 & 0 < \theta \leq \theta_h \\ E_w \dfrac{\theta - \theta_h}{\theta_w - \theta_h} & \theta_h < \theta \leq \theta_w \\ E_w + (ET_{max} - E_w)\dfrac{\theta - \theta_h}{\theta* - \theta_h} & \theta_w < \theta \leq \theta* \\ ET_{max} & \theta* < \theta \leq \varphi \end{cases}, \tag{9}$$

where E_w is soil evaporation, ET_{max} is maximum evapotranspiration, θ_h, θ_w, and θ^* are the hygroscopic, wilting and plant stress soil moisture thresholds, and φ is the soil porosity. Vivoni et al. (2008a) applied Eq. (9) to observations of ET from the EC method and θ at single locations to derive the relation parameters using a nonlinear optimiza-
5   tion algorithm (Gill et al., 1981). We evaluate this approach using the spatially-averaged soil moisture estimates (θ_{CRS} and θ_{SN}) whose spatial scale is more commensurate with the ET measurements. In addition, we combine Eq. (9) with Eqs. (7) and (8) to obtain analytical relations between evapotranspiration and the spatial variability of soil moisture, $ET = f(\sigma)$ and $ET = f(CV)$, and test these with θ_{CRS} and θ_{SN} observations.

10   3   Results and discussion

3.1   Comparison of CRS method to distributed sensor network

Figure 4 presents a comparison of the spatially-averaged, hourly soil moisture obtained from the CRS method (θ_{CRS}) and the distributed sensor network (θ_{SN}) during the study period. Relative to the long-term summer precipitation (Table 1), the study period had
15   below average (188 and 153 mm in 2013 and 2014) and significantly above average (246 and 247 mm) rainfall at SRER and JER, respectively. The fall-winter period in the record had below average precipitation (99 mm) at SRER and significantly below average amounts (21 mm) at JER. Overall, the spring periods were dry, consistent with the long-term averages. In response, the temporal variability of soil moisture clearly shows
20   the seasonal conditions at the two sites, with relatively wetter conditions during the summer monsoons. Seasonally-averaged θ_{CRS} compares favorably with seasonally-averaged θ_{SN} (Fig. 4), with both estimates showing large differences between wetter summer conditions (0.065 and 0.085 m^3 m^{-3} at SRER and JER) and drier spring values (0.028 and 0.021 m^3 m^{-3} at SRER and JER, respectively). As shown in prior studies
25   (e.g., Zreda et al., 2008; Franz et al., 2012b), the CRS method tracks very well the sensor observations. Nevertheless, there is an indication that θ_{CRS} has a tendency to

Title Page

Abstract | Introduction

Conclusions | References

Tables | Figures

◄ | ►

◄ | ►

Back | Close

Full Screen / Esc

Printer-friendly Version

Interactive Discussion

dry less quickly during some rainfall events (i.e., overestimate soil moisture during recession limbs), possibly due to landscape features such as nearby channels (Fig. 1) that remain wetter than areas measured by the distributed sensor network. Overall, however, there is an excellent match between θ_{CRS} and θ_{SN} in terms of capturing the occurrence and magnitude of soil moisture peaks across the different seasons, thus reducing some issues noted by Franz et al. (2012b) with respect to a purported oversensitivity of θ_{CRS} for small rainfall events (< 5 mm). We attribute this improvement primarily to including a 5 cm sensor in each profile that tracks the important soil moisture dynamics occurring in the shallow surface layer within semiarid ecosystems.

To complement this, Fig. 5 compares θ_{CRS} and θ_{SN} as a scatterplot along with the sample size (N) and the Standard Error of Estimates (SEE) which quantify the deviations from the 1 : 1 line. Table 3 provides the full set of statistical metrics for the comparison of θ_{CRS} versus θ_{SN} at the two study sites. The correspondence between both methods is excellent, with low RMSE and SEE, a high CC, and a Bias close to 1. These values are comparable to previous validation efforts where the RMSE was found to be 0.011 $m^3 m^{-3}$ (Franz et al., 2012b) and less than 0.03 $m^3 m^{-3}$ (Bogena et al., 2013; Coopersmith et al., 2014; Zhu et al., 2015). The comparison across the sites is also illustrative. Despite the more arid climate at JER (Table 1), the study period consisted of higher precipitation (247 mm) and higher soil moisture values during the summer (0.085 $m^3 m^{-3}$), as compared to SRER (170 mm, 0.065 $m^3 m^{-3}$), indicating a more active North American monsoon in the Chihuahuan Desert. In contrast, the fall-winter period is generally drier at JER (21 mm, 0.039 $m^3 m^{-3}$), as compared to SRER (99 mm, 0.057 $m^3 m^{-3}$), where high P and low ET in the winter promoted infiltration beyond the CRS measurement depth, as observed at a 1-m sensor profile at SRER (not shown). These two effects are observed as larger range of soil moisture values in Fig. 5 for JER. It is also worth noting that θ_{CRS} has a larger dynamic range for dry conditions (i.e., θ_{CRS} values can reach zero, whereas θ_{SN} does not), indicating that the method overcomes the measurement limitations discussed by Vereecken et al. (2014). Based on these comparisons, the CRS method is found to be a reliable approach for mea-

Water balance with cosmic-ray soil moisture data

A. P. Schreiner-McGraw et al.

Title Page

Abstract	Introduction
Conclusions	References
Tables	Figures

|◀ | ▶|

◀ | ▶

Back | Close

Full Screen / Esc

Printer-friendly Version

Interactive Discussion

suring intermediate scale soil moisture across the observed range of soil moistures at SRER and JER.

3.2 Comparison and analyses of CRS method and water balance estimates

Figure 6 presents the comparison of the spatially-averaged $\Delta\theta_{CRS}$ and $\Delta\theta_{WB}$ as a scatterplot for approximately 40 rainfall events larger than 10 mm, with statistical metrics shown in Table 3. The correspondence between the methods is very good, with low RMSE and SEE, a high CC, and a Bias close to 1, with a closer match at the SRER site. For example, the SEE at SRER ($0.020\,\mathrm{m^3\,m^{-3}}$) is about one half of the value at JER ($0.049\,\mathrm{m^3\,m^{-3}}$) and close to the SEE of the comparison of θ_{CRS} and θ_{SN}. This suggests that the three approaches for estimating soil moisture are in agreement at the SRER. For the JER, the lower correspondence between $\Delta\theta_{CRS}$ and $\Delta\theta_{WB}$ is attributed to five large events where $\Delta\theta_{WB}$ is above $0.2\,\mathrm{m^3\,m^{-3}}$. Removing these events lowers the SEE at JER to $0.020\,\mathrm{m^3\,m^{-3}}$, in line with SRER and the comparison of θ_{CRS} and θ_{SN} at JER. A closer inspection of the soil moisture response at JER is revealing. Figure 7 shows the soil moisture change ($\Delta\theta_{SN}$) at different sensor depths averaged for the selected large events and for remaining events, as well as the CRS measurement depths (z^*) for each case. The five large events exhibit high soil moisture changes at 30 cm depth (i.e., $0.08\,\mathrm{m^3\,m^{-3}}$) below z^* (i.e., 17 cm), while other events have soil moisture changes near zero at 30 cm and are captured well within z^*. This indicates that infiltration fronts during the larger events penetrated beyond z^* and were not entirely captured by the CRS method, leading to an underestimate of $\Delta\theta_{WB}$. In contrast, the better correspondence at SRER suggests that infiltration fronts were contained within z^* (see Table 3). This is plausible given the more homogeneous soil and flatter terrain at SRER as compared to JER (Anderson, 2013), where higher gravel contents, the presence of calcium carbonate and undulated terrain can promote soil water movement to deeper layers (Templeton et al., 2014).

To explore this further, Fig. 8 shows the cumulative f_{CRS} and the cumulative, spatially-averaged P and ET measured by the distributed sensor network. An overall drying trend is present at SRER during the study period (i.e., cumulative f_{CRS} becomes more negative), while JER exhibits a relatively small change in cumulative f_{CRS}, both in re-

5 sponse to the below average (SRER) and above average (JER) precipitation. An important contrast at the sites is the overall water balance (Table 4), where higher P, lower ET and lower Q at JER (measured ET $/ P = 0.54$, $Q / P = 0.01$) implies that more soil water is available for leakage to deeper soil layers. This is reflected in a large positive difference between cumulative outflow ($O = $ ET $+ L$) and ET at JER (i.e., $L > 0$ from z^*,

10 soil water movement to lower layers, as depicted in the soil water balance diagram). In contrast, SRER exhibits a higher ET $/ P = 0.96$ and $Q / P = 0.14$, such that negative differences occur between O and ET (i.e., $L < 0$ into z^*, movement from lower layers, as depicted in the soil water balance diagram). This is particularly important during the summers when vegetation is active and draws more ET than the outflow from the CRS

15 measurement depth, indicating that soil water is obtained from deeper soil layers that are readily accessed by velvet mesquite roots (e.g., Snyder and Williams, 2003; Scott et al., 2008; Potts et al., 2010). This is consistent with the sustained ET during inter-storm periods in the summer season at SRER despite the low θ_{CRS}, while JER exhibits sharp declines in ET when θ_{CRS} is reduced between storms.

20 Overall, the soil water balance from the CRS method shows stark ecosystem differences at the two sites during the study period. The mesquite savanna at SRER extracted substantial amounts of water from deeper soil layers during the summer season such that losses to runoff and the atmosphere are in excess of seasonal precipitation. It is likely that the deeper soil water is recharged beyond the CRS measurement depth

25 during winter periods (Scott et al., 2000) and subsequently accessed by deep-rooted trees during the summer (Scott et al., 2008). In contrast, the mixed shrubland at JER lost a substantial amount of precipitation to deeper soil layers throughout the year, due to the low values of runoff and evapotranspiration, and the soil, terrain and channel conditions promoting recharge (Templeton et al., 2014). Furthermore, the f_{CRS} approach

provided estimates that can be compared to the watershed water balance since these are at a similar spatial scale (Table 4). Estimates of outflow (O) from the measurement depth and leakage (L) are higher when calculated with θ_{SN}, consistent with more rapid drying as compared to the CRS method. On the other hand, the CRS method results in higher values of the runoff ratio (Q / P) than observed in the distributed sensor network, in particular for JER. This is likely due to the daily scale of the CRS analysis, which significantly limits the suitability of the runoff estimate for semiarid watersheds characterized by runoff responses lasting minutes to hours.

3.3 Soil moisture spatial variability within CRS footprint

Figure 9 depicts the relations between the absolute (σ) and relative (CV) spatial variability of soil moisture and the spatially-averaged conditions ($<\theta>$) derived from either θ_{SN} or θ_{CRS} at each study site. Least squares regressions of Eqs. (7) and (8) based on hourly observations were used to obtain k_1 and k_2, as shown in Table 5. For illustration purposes, bin-averages and standard deviations are also presented for each relation. As shown in prior efforts in semiarid ecosystems using sensor networks or aircraft observations (e.g., Fernández and Ceballos, 2003; Vivoni et al., 2008b; Mascaro et al., 2011), there is a general increase in σ with $<\theta>$ and a decrease of CV with $<\theta>$. The increase in spatial variability of soil moisture in absolute terms with wetter conditions is explained by the role played by local heterogeneities (e.g., vegetation types, surface soil variations, topography) as well as the bounded nature of the soil moisture process at the driest state (i.e., spatial variations are small in absolute terms when an area is very dry). Interestingly, both sites exhibit an asymptotic σ for the wettest values (above $0.1\,\mathrm{m^3\,m^{-3}}$ at SRER and $0.15\,\mathrm{m^3\,m^{-3}}$ at JER), as more clearly observed for θ_{SN}, indicating that the summer monsoon has wet soil moisture states that might be described as sub-humid, following the classification of Lawrence and Hornberger (2007). The observed relations of σ-$<\theta>$ and CV-$<\theta>$ at both sites are captured well by the exponential functions (Eqs. 7 and 8) leading to a low RMSE. Furthermore, a bootstrap analysis based on a random removal 100 points was conducted to generate

Water balance with cosmic-ray soil moisture data

A. P. Schreiner-McGraw et al.

Title Page

Abstract	Introduction
Conclusions	References
Tables	Figures

|◀ | ▶|

◀ | ▶

Back | Close

Full Screen / Esc

Printer-friendly Version

Interactive Discussion

95 % level confidence intervals for k_1 and k_2. We found that the set of k_1 and k_2 obtained for each site (Table 5) are included within the confidence intervals for both θ_{SN} or θ_{CRS}. This indicates the relations derived in these different sites might be broadly applicable to other semiarid ecosystems in the southwestern US. Nevertheless, there are some small discrepancies between the relations obtained for θ_{SN} and θ_{CRS} and the regressions parameters were shown to be significantly different at the 95 % confidence interval through a similar bootstrap analysis. We attribute these differences to the asymptotic behavior at the wettest states occurring after a rainfall event when θ_{CRS} has a slightly higher value than θ_{SN}, likely due to the instantaneous contribution of water above the ground surface (e.g., water in channels, surface depressions or on vegetation canopies).

3.4 Controls of Soil Moisture and Its Spatial Variability on Evapotranspiration

Figure 10 compares the relationships between the measured daily ET using the EC method and the spatially-averaged soil moisture values (θ_{SN} and θ_{CRS}) at the SRER and JER sites along with the piecewise linear regressions estimated using Eq. (9) and a nonlinear optimization approach. Following Vivoni et al. (2008a), regression parameters related to soil and vegetation conditions are presented in Table 6. For illustration purposes, bin-averages and standard deviations are also shown. Clearly, the piecewise linear relation is an excellent approach for capturing the ET-θ observations, yielding a relatively low RMSE at the two sites. A lower RMSE for the relation using θ_{CRS} as compared to θ_{SN} at SRER is attributed to its ability to detect a wider range of dry conditions and the improved match in the spatial scales of ET and θ_{CRS}, in an analogous fashion to the comparison between a single sensor and the distributed sensor network (Templeton et al., 2014). In addition, the CRS method represents soil evaporation (E_w) in a more realistic way as it discriminates differences in drier states. When comparing both sites through the ET-θ relation, the SRER has a larger E_w and ET_{max} and lower θ_*, as compared to JER, tested to be significantly different at the 95 % confidence level using a bootstrap approach. Together, these parameters indicate that SRER has a higher

overall ET, consistent with higher extractions from the CRS measurement depth due to the mesquite trees, extensive grass cover and higher soil evaporation.

We explore whether a daily relationship exists between the absolute (σ) and relative (CV) spatial variability of soil moisture and evapotranspiration in Fig. 11. Daily observations and bin-averages with standard deviations are derived entirely from the distributed sensor network and EC measurements. Given the relations linking σ and ET with the mean soil moisture (Figs. 9 and 10), the ET-σ relations exhibit an increase in ET with higher σ at both sites, though this is clearer at JER due to the wider range of θ_{SN}. This indicates that high absolute variability of soil moisture is associated with larger ET, likely due to the growth of wet patches supporting progressively more evapotranspiration. In contrast, the ET-CV relations exhibit a weaker negative trend such that a higher relative variability implies a lower ET. This occurs due to the role of the mean soil moisture state such that dry conditions have a relatively high CV (Fig. 9) and support a low ET (Fig. 10). Observations are compared to the analytical relations obtained by combining Eq. (9) with Eqs. (7) and (8) using θ_{CRS} as the spatially-averaged value for ET-σ and ET-CV, respectively (solid lines). While the analytical relations approximate the data fairly well, it is clear that the ET$_{max}$ limit (horizontal lines) does not represent the growth of ET with higher σ and lower CV. Nevertheless, the analytical functions are a promising application of the CRS method that can yield valuable information for understanding land-atmosphere interactions, under the assumption the σ-$<\theta>$ and ET-θ relations have been established (e.g., Tables 5 and 6).

4 Summary and conclusions

In this study, we utilized distributed sensor networks to examine the cosmic-ray sensing (CRS) soil moisture method at the small watershed scale in two semiarid ecosystems of the southwestern US (Pierini et al., 2014; Templeton et al., 2014). To our knowledge, this is the first study to compare CRS measurements to two complementary approaches for obtaining spatially-averaged soil moisture at a commensurate scale:

A. P. Schreiner-McGraw et al.

(1) a distributed set of sensor profiles weighted in the horizontal and vertical scales within each watershed, and (2) a watershed-averaged quantity obtained from closing the water balance. Coordinated efforts at the two small watersheds with varying landscape characteristics and precipitation conditions during the study period afforded the opportunity to conduct comparisons of soil moisture, evapotranspiration and vadose zone processes (infiltration, plant water uptake, leakage). We highlighted a few novel advantages of the CRS method revealed through the intercomparisons, including the ability to discriminate dry soil moisture states that is not possible through a sensor network, to resolve the shallow soil moisture dynamics captured well at the 5 cm sensors, and to match the independent soil moisture estimates from closing the water balance for most rainfall events. In the distributed sensor comparisons, we found that the CRS method overestimated the maximum soil moisture during rainfall events, likely due to the presence of water in surface depressions, plant canopies or channels. In the water balance comparisons, we identified that the CRS method was not able to capture the soil moisture conditions during large rainfall events and attributed this to rapid bypassing of the measurement depth promoted by watershed soil and terrain characteristics. Due to this observed bypass flow, we suggest that future seasonal water balance studies using the CRS method include a few soil moisture sensor profiles below z^* to detect leakage events.

We utilized the various measurement methods to explore the relative magnitudes of the water balance components at each site given the different precipitation amounts during the study period. The drier than average conditions in the mesquite savanna ecosystem at SRER lead to drier surface soils incapable of supporting the measured evapotranspiration unless supplemented by plant water uptake from deeper soil layers (Scott et al., 2008). In contrast, wetter than average summer periods in the mixed shrubland at JER had wet surface soils that promoted leakage into the deeper vadose zone which was subsequently unavailable for runoff and evapotranspiration losses (Duniway et al., 2010). Comparisons across different seasons at each site also suggested that carryover of soil water from winter leakage toward deeper soil layers is

consumed during the summer season by active plants. These novel inferences within the two ecosystems relied heavily on the application of the CRS method and its limited measurement depth to discriminate between shallow and deeper vadose zone processes as well as on the direct measurement of the water balance components, in particular evapotranspiration from the eddy covariance technique. It is important to keep in mind, however, that the ability to resolve watershed-scale hydrologic processes, such as the interaction between shallow and deep soil layers attributed to plant water uptake and leakage, depends to a large degree on the accuracy and representativeness of the distributed sensor network measurements and how their horizontal and vertical scales overlap with the CRS measurement footprint. We expect these limitations to be especially critical in semiarid ecosystems with high spatial heterogeneity induced by vegetation and bare soil patches.

The collocation of a distributed sensor network within the CRS measurement footprint allowed us to examine important process-based relations often incorporated into hydrologic models or remote sensing analyses (e.g., Famiglietti and Wood, 1994; Famiglietti et al., 2008). The spatial variability of soil moisture is linked to the spatially-averaged conditions through predictable relations that do not vary significantly across the study sites. For higher mean soil moisture, we observed a near linear increase in spatial variability followed by an asymptotic behavior attributed to the seasonally-wet conditions during the North American monsoon. Based on these relations (k_1 and k_2), the spatial variability within a CRS measurement footprint can be approximated for other semiarid ecosystems in the region. In addition, combining fixed and mobile CRS methods can establish landscape scale (10^2 to 10^3 km^2) soil moisture monitoring networks at grid sizes (~ 1 km^2) comparable to land surface modeling (Franz et al. 2015). Similarly, intermediate scale soil moisture sensing can be linked effectively to daily evapotranspiration and used to obtain soil and vegetation parameters (E_w, ET$_{max}$, θ_h, θ_w, and θ^*) tailored to each ecosystem. In term of the ET-θ relation, the CRS method has the potential to significantly improve land-atmosphere interaction studies through the commensurate scale achieved to the EC technique. Furthermore, we found

Full Screen / Esc

Printer-friendly Version

Interactive Discussion

that analytical relations linking soil moisture spatial variability with evapotranspiration exhibit similar characteristics to the observed datasets. As the spatial variability in soil moisture grows in the two semiarid ecosystems there is a concomitant increase in evapotranspiration. While this suggests that wet patches in a drier background sustain higher atmospheric losses, further investigations are needed to disentangle the individual roles of soil evaporation and plant water uptake on setting both the soil moisture spatial variability and the resulting evapotranspiration averaged in its measurement footprint.

References

Anderson, C. A.: Assessing land-atmosphere interactions through distributed footprint sampling at two eddy covariance towers in semiarid ecosystems of the southwestern U.S, Masters of Science in Civil, Environmental and Sustainable Engineering, Arizona State University, 243 pp., 2013.

Bindlish, R., Crow, W. T., and Jackson, T. J.: Role of passive microwave remote sensing in improving flood forecasts, IEEE Geosci. Remote Sens. Lett., 6, 112–116, 2009.

Bogena, H. R., Huisman, J. A., Baatz, R., Franssen, H. J. H., and Vereecken, H.: Accuracy of the cosmic-ray soil water content probe in humid forest ecosystems: The worst case scenario, Water Resour. Res., 49, 5778–5791, 2013.

Browning, D. M., Franklin, J., Archer, S. R., Gillan, J. K., and Guertin, D. P.: Spatial patterns of grassland-shrubland state transitions: a 74-year record on grazed and protected areas, Ecol. Appl., 24, 1421–1433, 2014.

Campbell, J. E.: Dielectric properties and influence of conductivity in soils at one to fifty Megahertz, Soil Sci. Soc. Am. J., 54, 332–341, 1990.

Full Screen / Esc

Printer-friendly Version

Interactive Discussion

Chen, F., Mitchell, K., Schaake, J., Xue, Y., Pan, H.-L., Koren, V., Duan, Q. Y., Ek, M., and Betts, A.: Modeling of land surface evaporation by four schemes and comparisons with FIFE observations, J. Geophys. Res., 101, 7251–7268, 1996.

Coopersmith, E. J., Cosh, M. H., and Daughtry, C. S. T.: Field-scale moisture estimates using COSMOS sensors: A validation study with temporary networks and Leaf-Area-Indices, J. Hydrol., 519, 637–643, 2014.

Dane, J. H. and Topp, C. G.: Methods of soil analysis. Part 4. Physical methods, SSSA Book Ser. 5. SSSA, Madison, WI, 2002.

Desilets, D. and Zreda, M.: Spatial and temporal distribution of secondary cosmic-ray nucleon intensities and applications to in-situ cosmogenic dating, Earth Planet. Sci. Lett., 206, 21–42, 2003.

Desilets, D. and Zreda, M.: Footprint diameter for a cosmic-ray soil moisture probe: Theory and Monte Carlo simulations, Water Resour. Res., 49, 3566–3575, 2013.

Desilets, D., Zreda, M., and Ferré, T. P. A.: Nature's neutron probe: Land surface hydrology at an elusive scale with cosmic rays, Water Resour. Res., 46, W11505, doi:10.1029/2009WR008726, 2010.

Dugas, W. A., Hicks, R. A., and Gibbens, R. P.: Structure and function of C3 and C4 Chihuahuan Desert plant communities: Energy balance components, J. Arid Environ., 34, 63–79, 1996.

Duniway, M. C., Snyder, K. A., and Herrick, J. E.: Spatial and temporal patterns of water availability in a grass-shrub ecotone and implications for grassland recovery in arid environments, Ecohydrology, 3, 55–67, 2010.

Eltahir, E. A. B.: A soil moisture rainfall feedback mechanism 1. Theory and observations. Water Resour. Res., 34, 765–776, 1998.

Entekhabi, D.: Recent advances in land-atmosphere interaction research. Reviews of Geophysics, 33, 995–1004, 1995.

Falge, E., Baldocchi, D., Tenhunen, J., Aubinet, M., Bakwin, P., Berbigier, P., Bernhofer, C., Burba, G., Clement, R., Davis, K. J., Elbers, J. A., Goldstein, A. H., Grelle, A., Granier, A., Gudmundsson, J., Hollinger, D., Kowalski, A. S., Katul, G., Law, B. E., Malhi, Y., Meyers, T., Monson, R. K., Munger, J. W., Oechel, W., Paw, K. T., Pilegaard, K., Rannik, U., Rebmann, C., Suyker, A., Valentini, R., Wilson, K., and Wofsy, S.: Seasonality of ecosystem respiration and gross primary production as derived from FLUXNET measurements, Agricult. Forest Meteorol., 113, 53–74, 2002.

Water balance with cosmic-ray soil moisture data

A. P. Schreiner-McGraw et al.

Fernández, J. M. and Ceballos, A.: Temporal stability of soil moisture in a large-field experiment in Spain, Soil Sci. Soc. Am. J., 67, 1647–1656, 2003.

Famiglietti, J. S. and Wood, E. F.: Multiscale modeling of spatially variable water and energy balance processes, Water Resour. Res., 30, 3061–3078, 1994.

Famiglietti, J. S., Devereaux, J. A., Laymon, C. A., Tsegaye, T., Houser, P. R., Jackson, T. J., Graham, S. T., Rodell, M., and van Oevelen, P. J.: Ground-based investigation of soil moisture variability within remote sensing footprints during the Southern Great Plains 1997(SGP97) Hydrology Experiment, Water Resour. Res., 35, 1839–1851, 1999.

Famiglietti, J. S., Ryu, D., Berg, A. A., Rodell, M., and Jackson, T. J.: Field observations of soil moisture variability across scales. Water Resour. Res., 44, W01423, doi:10.1029/2006WR005804, 2008.

Franz, T. E., Zreda, M., Ferré, T. P. A., Rosolem, R., Zweck, C., Stillman, S., Zeng, X., and Shuttleworth, W. J.: Measurement depth of the cosmic-ray soil moisture probe affected by hydrogen from various sources, Water Resour. Res., 48, W08515, doi:10.1029/2012WR011871, 2012a.

Franz, T. E., Zreda, M., Rosolem, R., and Ferré, T. P. A.: Field validation of a cosmic-ray neutron sensor using a distributed sensor network, Vadose Zone J., 11, doi:10.2136/vzj2012.0046, 2012b.

Franz, T. E., Zreda, M., Rosolem, R., Hornbuckle, B. K., Irvin, S. L., Adams, H., Kolb, T. E., Zweck, C., and Shuttleworth, W. J.: Ecosystem-scale measurements of biomass water using cosmic ray neutrons, Geophys. Res. Lett., 40, 3929–3933, 2013a.

Franz, T. E., Zreda, M., Ferré, T. P. A., and Rosolem, R.: An assessment of the effect of horizontal soil moisture heterogeneity on the area-average measurement of cosmic-ray neutrons, Water Resour. Res., 49, 6450–6458, 2013b.

Franz, T. E., Wang, T., Avery, W., Finkenbiner, C., and Brocca, L.: Combined analysis of soil moisture measurements from roving and fixed cosmic ray neutron probes for multiscale real-time monitoring, Geophys. Res. Lett., 42, 3389–3396, doi:10.1002/2015GL063963, 2015.

Gardner, W. H. and Kirkham, D.: Determination of soil moisture by neutron scattering, Soil Science, 73, 391–401, 1952.

Gibbens, R. P. and Beck, R. F.: Increase in number of dominant plants and dominance-classes on a grassland in the northern Chihuahuan Desert, J. Range Manage., 40, 136–139, 1987.

Gill, P. E., Murray, W., and Wright, M. H.: Practical Optimization, Academic Press, London, UK, 402 pp., 1981.

Glasstone, S. and M. C. Edlund: Elements of Nuclear Reactor Theory, Van Nostrand, New York, 416 pp., 1952.

Greacen, E. L.: Soil Water Assessment by the Neutron Method, CSIRO, Melbourne, Australia, 148 pp., 1981.

Gutiérrez-Jurado, H. A., Vivoni, E. R., Cikoski, C., Harrison, J. B. J., Bras, R. L., and Istan-bulluoglu, E. I.: On the observed ecohydrologic dynamics of a semiarid basin with aspect-delimited ecosystems, Water Resour. Res., 49, 8263–8284, 2013.

Hsieh C.-I., Katul, G., and Chi, T.: An approximate analytical model for footprint estimation of scalar fluxes in thermally stratified atmospheric flows, Adv. Water Res., 23, 765–772, 2000.

Huang, C., March, S. E., McClaran, M. P., and Archer, S. R.: Postfire stand structure in a semiarid savanna: cross-scale challenges estimating biomass, Ecol. Appl., 17, 1899–1910, 2007.

Huenneke, L. F., Clason, D., and Muldavin, E.: Spatial heterogeneity in Chihuahuan Desert vegetation: implications for sampling methods in semi-arid ecosystems, J. Arid Environ., 47, 257–270, 2001.

Ivanov, V. Y., Vivoni, E. R., Bras, R. L., and Entekhabi, D.: Catchment hydrologic response with a fully-distributed triangulated irregular network model, Water Resour. Res., 40, W11102, doi:10.1029/2004WR003218, 2004.

Kormann, R. and Meixner, F. X.: An analytical footprint model for non-neutral stratification, Bound. Layer Meteorol., 99, 207–224, 2001.

Kustas, W. P., Zhan, X., and Schmugge, T. J.: Combining optical and microwave remote sensing for mapping energy fluxes in a semiarid watershed, Remote Sens. Environ., 64, 116–131, 1998.

Laio, F., Porporato, A., Ridolfi, L., and Rodríguez-Iturbe, I.: Plants in water-controlled ecosystems: active role in hydrologic processes and response to water stress II, Probabilistic soil moisture dynamics, Adv. Water Res., 24, 707–723, 2001.

Lawrence, J. E. and Hornberger, G. M.: Soil moisture variability across climate zones, Geophys. Res. Lett., 34, L20402, doi:10.1029/2007GL031382, 2007.

Mascaro, G. and Vivoni, E. R.: Utility of coarse and downscaled soil moisture products at L-band for hydrologic modeling at the catchment scale, Geophys. Res. Lett., 39, L10403, doi:10.1029/2012GL051809, 2012.

Title Page

Abstract | Introduction

Conclusions | References

Tables | Figures

◄ | ►

◄ | ►

Back | Close

Full Screen / Esc

Printer-friendly Version

Interactive Discussion

Mascaro, G., Vivoni, E. R., and Deidda, R.: Soil moisture downscaling across climate regions and its emergent properties, J. Geophys. Res., 116, D22114, doi:10.1029/2011JD016231, 2011.

McJannet, D., Franz, T. E., Hawdon, A., Boadle, D., Baker, B., Almeida, A., Silberstein, R., Lambert, T., and Desilets, D.: Field testing of the universal calibration function for determination of soil moisture with cosmic-ray neutrons, Water Resour. Res., 50, 5235–5248, 2014.

Moran, M. S., Hymer, D. C., Qi, J. G., and Sano, E. E.: Soil moisture evaluation using multi-temporal synthetic aperture radar (SAR) in semiarid rangeland, Agricult. Forest Meteorol., 105, 69–80, 2000.

Narayan, U. and Lakshmi, V.: Characterizing subpixel variability of low resolution radiometer derived soil moisture using high resolution radar data, Water Resour. Res., 44, W06425, doi:10.1029/2006WR005817, 2008.

Pierini, N. A.: Exploring the ecohydrological impacts of woody plant encroachment in paired watersheds of the Sonoran Desert, Arizona. Master of Science Thesis in Civil, Environmental and Sustainable Engineering, Arizona State University, Tempe, AZ, 160 pp., 2013.

Pierini, N. P., Vivoni, E. R., Robles-Morua, A., Scott, R. L., and Nearing, M. A.: Using observations and a distributed hydrologic model to explore runoff thresholds linked with mesquite encroachment in the Sonoran Desert, Water Resour. Res., 50, doi:10.1002/2014WR015781, 2014.

Polyakov, V. O., Nearing, M. A., Nichols, M. H., Scott, R. L., Stone, J. J., and McClaran, M. P.: Long-term runoff and sediment yields from small semiarid watersheds in southern Arizona. Water Resour. Res., 46, W09512, doi:10.1029/2009WR009001, 2010.

Potts, D. L., Scott, R. S., Bayram, S., and Carbonara, J.: Woody plants modulate the temporal dynamics of soil moisture in a semi-arid mesquite savanna, Ecohydrology, 3, 20–27, 2010.

Rodríguez-Iturbe, I. and Porporato, A.: Ecohydrology of Water-Controlled Ecosystems, Cambridge Univ. Press, Cambridge, UK, 442 pp., 2004.

Rosolem, R., Shuttleworth, W. J., Zreda, M., Franz, T., Zeng, X., and Kurc, S. A.: The effect of atmospheric water vapor on neutron count in the cosmic-ray soil moisture observing system, J. Hydrometeorol., 14, 1659–1671, 2013.

Scott, R. L.: Using watershed water balance to evaluate the accuracy of eddy covariance evaporation measurements for three semiarid ecosystems, Agricult. Forest Meteorol., 150, 219–225, 2010.

Water balance with cosmic-ray soil moisture data

A. P. Schreiner-McGraw et al.

Title Page

Abstract | Introduction

Conclusions | References

Tables | Figures

|◀ | ▶|

◀ | ▶

Back | Close

Full Screen / Esc

Printer-friendly Version

Interactive Discussion

Scott, R. L., Shuttleworth, W. J., Keefer, T. O., and Warrick, A. W.: Modeling multi-year observations of soil moisture recharge in the semiarid American Southwest, Water Resour. Res., 36, 2233–2247, 2000.

Scott, R. L., Edwards, E. A., Shuttleworth, W. J., Huxman, T. E., Watts, C., and Goodrich, D. C.: Interannual and seasonal variation in fluxes of water and carbon dioxide from a riparian woodland ecosystem, Agricult. Forest Meteorol., 122, 65–84, 2004.

Scott, R. L., Huxman, T. E., Williams, D. G., and Goodrich, D. C.: Ecohydrological impacts of woody-plant encroachment: seasonal patterns of water and carbon dioxide exchange within a semiarid riparian environment, Global Change Biol., 12, 311–324, 2006.

Scott, R. L., Cable, W. L., and Hultine, K. R.: The ecohydrologic significance of hydraulic redistribution in a semiarid savanna, Water Resour. Res., 44, W02440, doi:10.1029/2007WR006149, 2008.

Seyfried, M. S., Grant, L. E., Du, E., and Humes, K.: Dielectric loss and calibration of the Hydra probe soil water sensor, Vadose Zone J., 4, 1070–1079, 2005.

Small, E. E. and Kurc, S. A.: Tight coupling between soil moisture and the surface radiation budget in semiarid environments: Implications for land-atmosphere interactions. Water Resour. Res., 39, 1278, doi:10.1029/2002WR00129, 2003 .

Smith, R. E., Chery, D. L., Renard, K. G., and Gwinn, W. R.: Supercritical flow flumes for measuring sediment-laden flow, Tech. Bull., US Gov. Print. Off., Washington, D.C., 1655, 70 pp., 1981.

Snyder, K. A. and Williams, D. G.: Defoliation alters water uptake by deep and shallow roots of *Prosopis velutina* (velvet mesquite), Funct. Ecol., 17, 363–374, 2003.

Stillman, S., Ninneman, J., Zeng, X., Franz, T., Scott, R. L., Shuttleworth, W. J., and Cummins, K.: Summer soil moisture spatiotemporal variability in southeastern Arizona, J. Hydrometeorol., 15, 1473–1485, 2014.

Templeton, R. C., Vivoni, E. R., Méndez-Barroso, L. A., Pierini, N. A., Anderson, C. A., Rango, A., Laliberte, A. S., and Scott, R. L.: High-resolution characterization of a semiarid watershed: Implications on evapotranspiration estimates, J. Hydrol., 509, 306–319, 2014.

Throop, H.L., Archer, S. R., Monger, H. C., and Waltman, S.: When bulk density methods matter: Implications for estimating soil organic carbon pools in rocky soils, J. Arid Environ., 77, 66–71, 2011.

Topp, G. C., Davis, J. L., and Annan, A. P.: Electromagnetic determination of soil water content: Measurements in coaxial transmission lines, Water Resour. Res., 16, 574–582, 1980.

Title Page

Abstract | Introduction

Conclusions | References

Tables | Figures

◄ | ►

◄ | ►

Back | Close

Full Screen / Esc

Printer-friendly Version

Interactive Discussion

Turnbull, L., Parsons, A. J., and Wainwright, J.: Runoff responses to long-term rainfall variability in creosotebush-dominated shrubland, J. Arid Environ., 91, 88–94, 2013.

Vereecken, H., Huisman, J. A., Pachepsky, Y., Montzka, C., van der Kruk, J., Bogena, H., Weihermuller, L., Herbst, M., Martinez, G., and Vanderborght, J.: On the spatio-temporal dynamics of soil moisture at the field scale, J. Hydrol., 516, 76–96, 2014.

Vivoni, E. R.: Spatial patterns, processes and predictions in ecohydrology: Integrating technologies to meet the challenge, Ecohydrology, 5, 235–241, 2012.

Vivoni, E. R., Moreno, H. A., Mascaro, G., Rodríguez, J. C., Watts, C. J., Garatuza-Payán, J., and Scott, R. L.: Observed relation between evapotranspiration and soil moisture in the North American monsoon region, Geophys. Res. Lett., 35, L22403, doi:10.1029/2008GL036001, 2008a.

Vivoni, E. R., Gebremichael, M., Watts, C. J., Bindlish, R., and Jackson, T. J.: Comparison of ground-based and remotely-sensed surface soil moisture estimates over complex terrain during SMEX04, Remote Sens. Environ., 112, 314–325, 2008b.

Vivoni, E. R., Rango, A., Anderson, C. A., Pierini, N. A., Schreiner-McGraw, A. P., Saripalli, S., and Laliberte, A. S.: Ecohydrology with unmanned aerial vehicles, Ecosphere 5, 130, doi:10.1890/ES14-00217.1, 2014.

Western, A. W., Grayson, R. B., and Blöshl, G.: Scaling of soil moisture: A hydrologic perspective, Ann. Rev. Earth Planet. Sci., 30, 149–180, 2002.

Wilson, K., Goldstein, A., Falge, E., Aubinet, M., Baldocchi, D., Berbigier, P., Bernhofer, C., Ceulemans, R., Dolman, H., Field, C., Grelle, A., Ibrom, A., Law, B. E., Kowalski, A., Meyers, T., Moncrieff, J., Monson, R., Oechel, W., Tenhunen, J., Valentini, R., and Verma, S.: Energy balance closure at FLUXNET sites, Agricult. Forest Meteorol., 113, 223–243, 2002.

Zhu, Z., Tan, L., Gao, S., and Jiao, Q.: Observation on soil moisture of irrigation cropland by cosmic-ray probe, IEEE Geosci. Remote Sens. Lett., 12, 472–476, doi:10.1109/LGRS.2014.2346784, 2015.

Zreda, M., Desilets, D., Ferre, T. P. A., and Scott, R. L.: Measuring soil moisture content non-invasively at intermediate spatial scale using cosmic-ray neutrons, Geophys. Res. Lett., 35, L21402, doi:10.1029/2008GL035655, 2008.

Zreda, M., Shuttleworth, W. J., Zeng, X., Zweck, C., Desilets, D., Franz, T., and Rosolem, R.: COSMOS: the COsmic-ray Soil Moisture Observing System, Hydrol. Earth Syst. Sci., 16, 4079–4099, doi:10.5194/hess-16-4079-2012, 2012.

Title Page

Abstract | Introduction

Conclusions | References

Tables | Figures

◄◄ | ►►

◄ | ►

Back | Close

Full Screen / Esc

Printer-friendly Version

Interactive Discussion

Table 1. Watershed and precipitation characteristics at the SRER and JER sites. Precipitation values are long-term averages (1923–2014 at SRER and 1915–2006 at JER) for annual and seasonal quantities, defined as fall (October-December), winter (January–March), spring (April–June) and summer (July–September).

Characteristic (unit)	Value	SRER	JER
Watershed area (m^2)		12 535	46734
Elevation (m)	mean	1166.6	1458.3
	max	1171.1	1467.5
	min	1160.9	1450.5
Slope (degree)	mean	3.2	3.9
	max	19.2	45
	min	2.1	0
Drainage density (1/m)		0.04	0.03
Major vegetation type (%)	shrubs	32 %	27 %
	cacti	6 %	1 %
	grasses	37 %	6 %
	bare soil	25 %	66 %
Precipitation (mm)	annual	364	251
	fall	72	54
	winter	69	31
	spring	26	32
	summer	197	134

Table 2. Energy balance closure at SRER and JER using 30 min net radiation (R_n), ground (G), latent (λE) and sensible (H) heat fluxes. The parameters m and b are the slope and intercept in the relation $\lambda E + H = m(R_n - G) + b$, while the ratio of the sum of ($\lambda E + H$) to the sum of ($R_n - G$) is a measure of how much available energy is accounted for in the turbulent fluxes.

Site	$\lambda E + H = m(R_n G) + b$		$\frac{\sum \lambda E + H}{\sum R_n - G}$
	m	b	
SRER	0.72	17	0.85
JER	0.72	9.9	0.82

Table 3. Statistical comparisons of CRS method with distributed sensor network and water balance estimates based on the Standard Error of Estimates, $\mathrm{SEE} = \sqrt{\frac{\sum(\theta_{\mathrm{SN}} - \theta_{\mathrm{CRS}})^2}{N}}$, Root Mean Square Error, $\mathrm{RMSE} = \sqrt{\frac{\sum(\theta'_{\mathrm{CRS}} - \theta_{\mathrm{CRS}})^2}{N}}$ where θ'_{CRS} is the predicted value of θ_{CRS} based on the best fit line with θ_{SN}, Bias, $B = \frac{\overline{\theta_{\mathrm{CRS}}}}{\overline{\theta_{\mathrm{SN}}}}$ and Correlation Coefficient, $\mathrm{CC} = \frac{\sum\limits_{i=1}^{N}\left(\theta_{\mathrm{CRS},i} - \overline{\theta_{\mathrm{CRS}}}\right)\left(\theta_{\mathrm{SN},i} - \overline{\theta_{\mathrm{SN}}}\right)}{\left[\sum\limits_{i=1}^{N}\left(\theta_{\mathrm{CRS},i} - \overline{\theta_{\mathrm{CRS}}}\right)^2\right]^{0.5}\left[\sum\limits_{i=1}^{N}\left(\theta_{\mathrm{SN},i} - \overline{\theta_{\mathrm{SN}}}\right)^2\right]^{0.5}}$ where $\overline{\theta_{\mathrm{CRS}}}$ and $\overline{\theta_{\mathrm{SN}}}$ represent the mean soil moisture for each measurement method and N is the number of samples. Values in parentheses for JER indicate metrics when large rainfall events are excluded.

Metric (unit)	SRER	JER
θ_{CRS} versus θ_{SN}		
RMSE ($\mathrm{m^3\,m^{-3}}$)	0.009	0.013
CC	0.949	0.946
B	1.117	1.019
SEE ($\mathrm{m^3\,m^{-3}}$)	0.012	0.013
$\Delta\theta_{\mathrm{CRS}}$ versus $\Delta\theta_{\mathrm{WB}}$		
RMSE ($\mathrm{m^3\,m^{-3}}$)	0.001	0.038 (0.019)
CC	0.954	0.945 (0.946)
B	1.167	0.702 (0.903)
SEE ($\mathrm{m^3\,m^{-3}}$)	0.020	0.049 (0.020)

Title Page

Abstract · Introduction

Conclusions · References

Tables · Figures

|◄ · ►|

◄ · ►

Back · Close

Full Screen / Esc

Table 4. Total water flux estimates from daily CRS soil water balance method (f_{CRS}) and daily sensor measurements during study period at the SRER and JER sites. P is from rain gauge measurements in both cases. L in CRS is computed as O − ET where ET is from EC method, while L in sensor estimates is calculated from solving the water balance.

Water flux	SRER	JER
CRS estimates		
Precipitation (P, mm)	464	533
Infiltration (I, mm)	357	477
Outflow (O, mm)	391	482
Leakage (L, mm)	−56	193
Outflow ratio (O / P)	0.84	0.90
Runoff ratio (Q / P)	0.23	0.11
Sensor estimates		
Precipitation (P, mm)	464	533
Storage change ($\Delta\theta$, mm)	−13	26
Outflow (O, mm)	437	506
Leakage (L, mm)	−10	217
Evapotranspiration (ET, mm)	447	289
Evaporation ratio (ET $/ P$)	0.96	0.54
Outflow ratio (O / P)	0.94	0.95
Streamflow (Q, mm)	64	5
Runoff ratio (Q / P)	0.14	0.01

Title Page

Abstract | Introduction

Conclusions | References

Tables | Figures

|◀ | ▶|

◀ | ▶

Back | Close

Full Screen / Esc

Printer-friendly Version

Interactive Discussion

Table 5. Regression parameters for the relations of the spatial variability of soil moisture (σ and CV) and $<\theta>$ at the SRER and JER sites along with the RMSE of the regressions.

Relation	SRER			JER		
	k_1	k_2	RMSE	k_1	k_2	RMSE
$\sigma - \theta_{SN}$	0.75	4.23	$0.007\,\mathrm{m^3\,m^{-3}}$	0.74	2.75	$0.005\,\mathrm{m^3\,m^{-3}}$
$\sigma - \theta_{CRS}$	0.57	1.80	$0.007\,\mathrm{m^3\,m^{-3}}$	0.65	1.81	$0.007\,\mathrm{m^3\,m^{-3}}$
CV - θ_{SN}	0.78	5.40	0.145	0.72	2.48	0.067
CV - θ_{CRS}	0.87	6.36	0.020	0.72	2.24	0.071

Table 6. Regression parameters for the relations of evapotranspiration and soil moisture (θ_{SN} and θ_{CRS}) at the SRER and JER sites along with the RMSE of the regressions. $\theta_h = 0$ in all cases.

Site	Relation	ET_{max} (mm d^{-1})	E_w (mm d^{-1})	θ_w (m^3 m^{-3})	θ^* (m^3 m^{-3})	RMSE (mm d^{-1})
SRER	ET-θ_{SN}	2.61	0.41	0.03	0.07	1.15
	ET-θ_{CRS}	2.40	0.36	0.02	0.08	0.55
JER	ET-θ_{SN}	2.16	0.18	0.03	0.12	0.34
	ET-θ_{CRS}	2.17	0.21	0.03	0.13	0.34

Full Screen / Esc
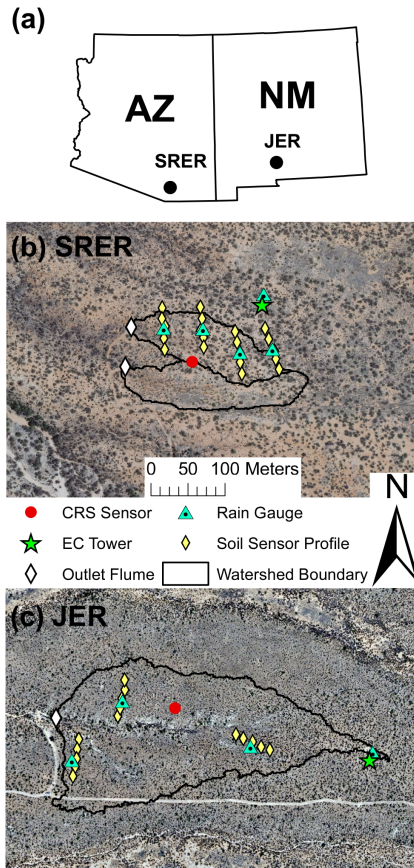
Figure 1. (a) Location of the study sites in Arizona and New Mexico. Watershed representations and sensor locations at **(b)** SRER and **(c)** JER, shown at the same scale.
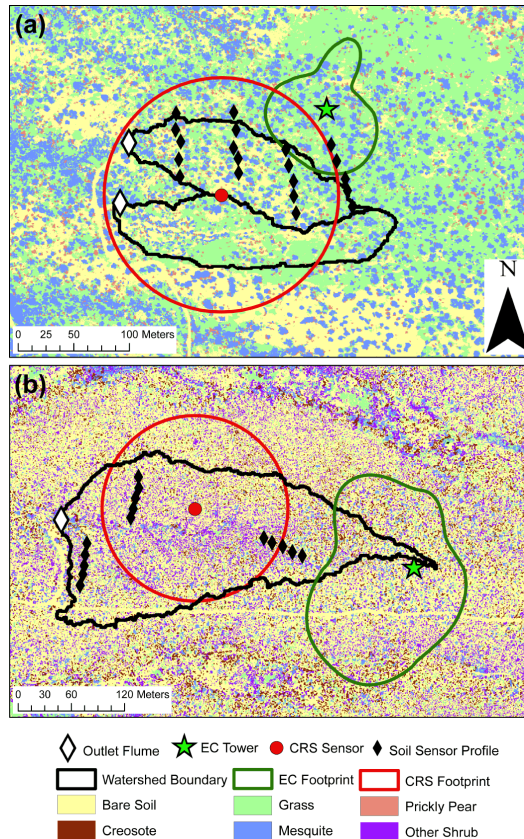
Figure 2. Vegetation classification for **(a)** SRER and **(b)** JER derived from aerial image analyses along with sensor locations and the 50 % contributing areas of the CRS and EC footprints.
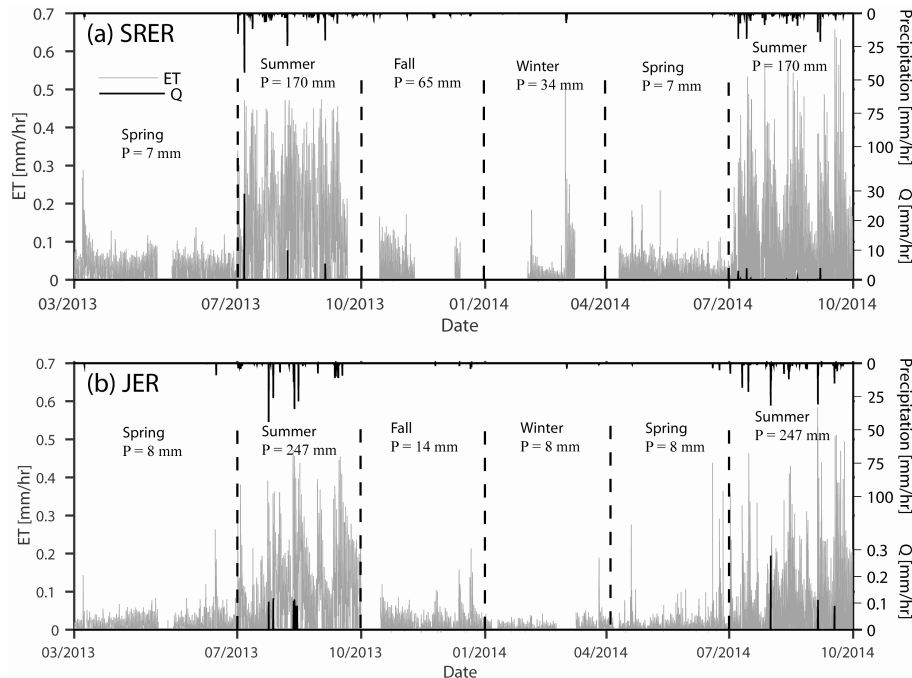
Figure 3. Hourly precipitation, streamflow and evapotranspiration at the **(a)** SRER and **(b)** JER sites during the study period (March 2013 to September 2014). Gaps in ET data indicate periods of EC tower malfunction due to equipment failures, data collection problems or vandalism. Vertical dashed lines indicate the seasonal definitions and their corresponding total precipitation.
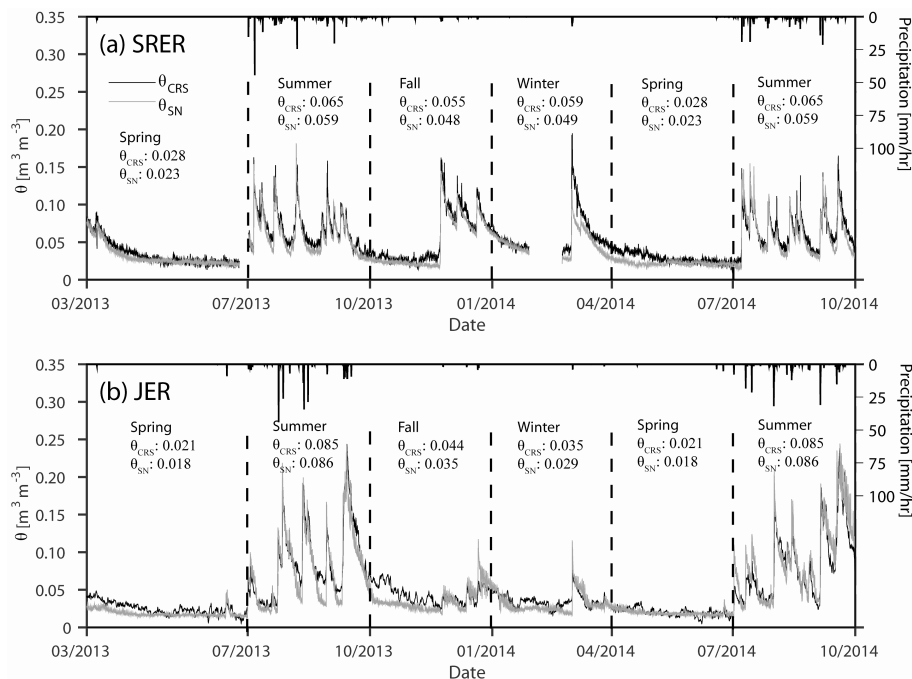
Figure 4. Comparison of the spatially-averaged, hourly soil moisture (m^3 m^{-3}) from CRS method (θ_{CRS}, black lines) and distributed sensor network (θ_{SN}, gray lines) at **(a)** SRER and **(b)** JER, along with spatially-averaged, hourly precipitation during 1 March 2013 to 30 September 2014. Vertical dashed lines indicate the seasonal definitions and their corresponding seasonally-averaged θ_{CRS} and θ_{SN} in m^3 m^{-3}.

Title Page

Abstract | Introduction

Conclusions | References

Tables | Figures

◄ | ►

◄ | ►

Back | Close

Full Screen / Esc
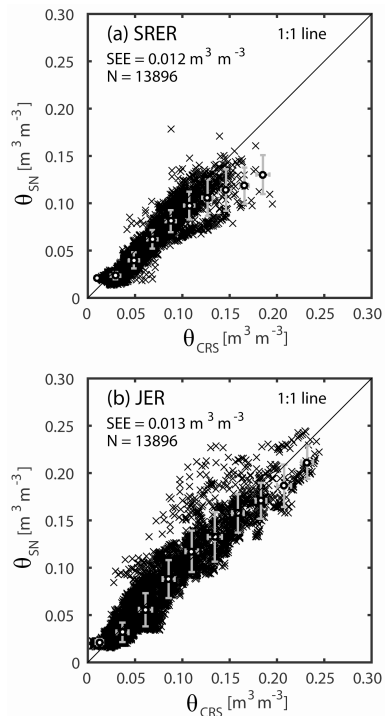
Figure 5. Scatterplots of the spatially-averaged, hourly soil moisture ($m^3\,m^{-3}$) from CRS method (θ_{CRS}) and distributed sensor network (θ_{SN}) at **(a)** SRER and **(b)** JER. The SEE and the number of hourly samples (N) are shown for each site. Bin averages and ± 1 standard deviation are shown (circles and error bars) for bin widths of $0.025\,m^3\,m^{-3}$ for each estimate.

Full Screen / Esc

Printer-friendly Version

Interactive Discussion
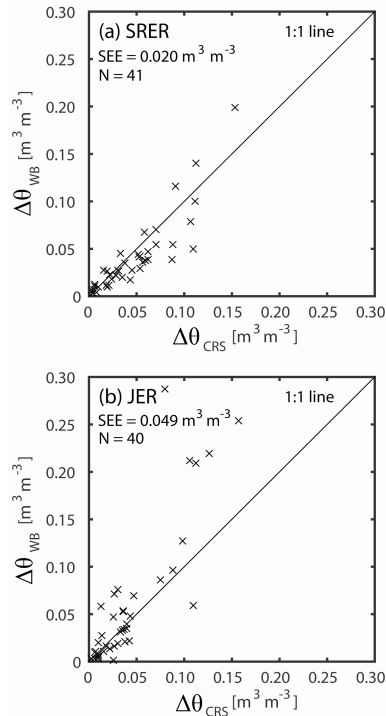
Figure 6. Scatterplots of the spatially-averaged change in soil moisture ($m^3 m^{-3}$) derived from CRS method ($\Delta\theta_{CRS}$) and the application of the water balance ($\Delta\theta_{WB}$) at **(a)** SRER and **(b)** JER. The SEE and the number of event samples (N) are shown for each site.

Title Page

Abstract | Introduction

Conclusions | References

Tables | Figures

|◄ | ►|

◄ | ►

Back | Close

Full Screen / Esc

Printer-friendly Version

Interactive Discussion
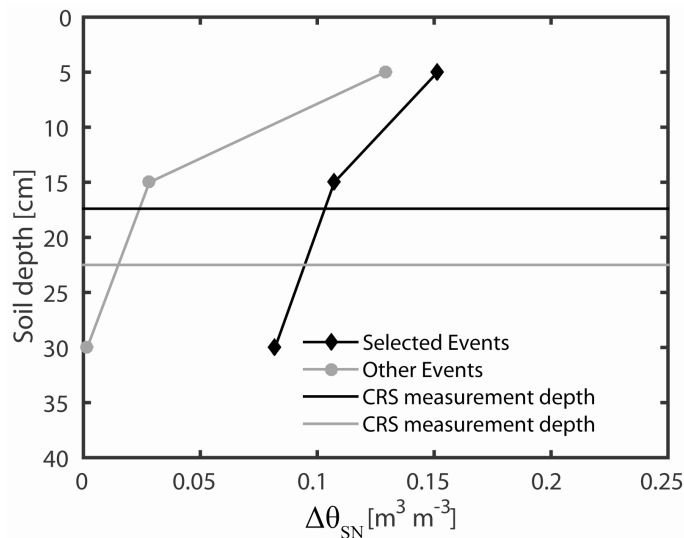
Figure 7. Change in soil moisture ($\Delta\theta_{SN}$) at depths of 5, 15 and 30 cm at the JER for the five large events ("Selected Events") and the remaining ("Other Events") cases. Horizontal lines are the CRS measurement depths averaged over the corresponding cases (black is Selected Events, gray is Other Events).
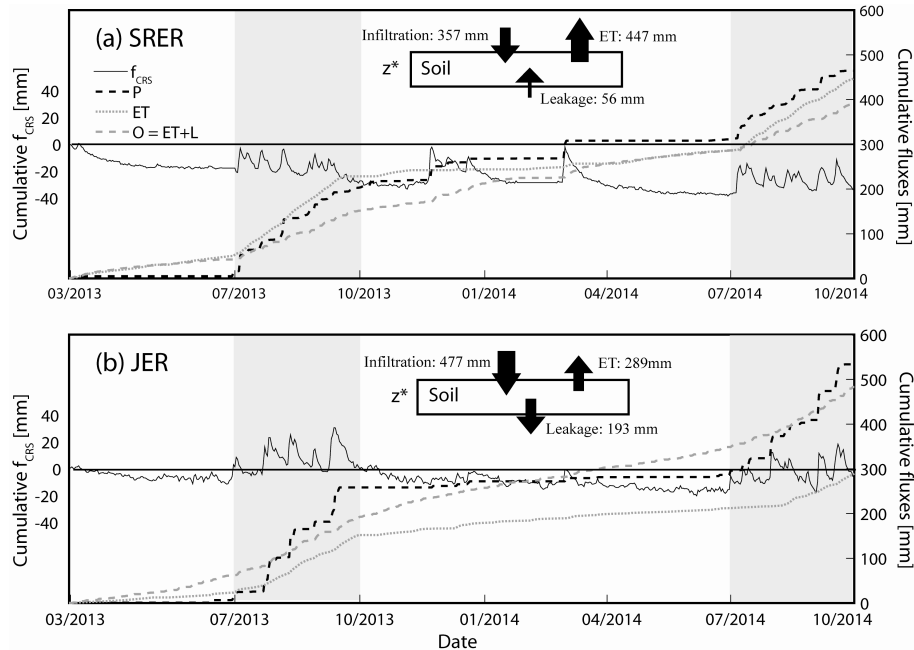
Figure 8. Comparison of cumulative f_{CRS} and measured water balance fluxes (P and ET) during study period. CRS estimates of infiltration (I), outflow (O) and leakage (L) are either depicted as cumulative fluxes ($O = ET + L$) or as total amounts during the study period (I and L) as arrows in the soil water balance box of depth z^*. Shaded regions indicate the summer seasons (July–September). The horizontal line represents $f_{CRS} = 0$.

Full Screen / Esc

Printer-friendly Version

Interactive Discussion
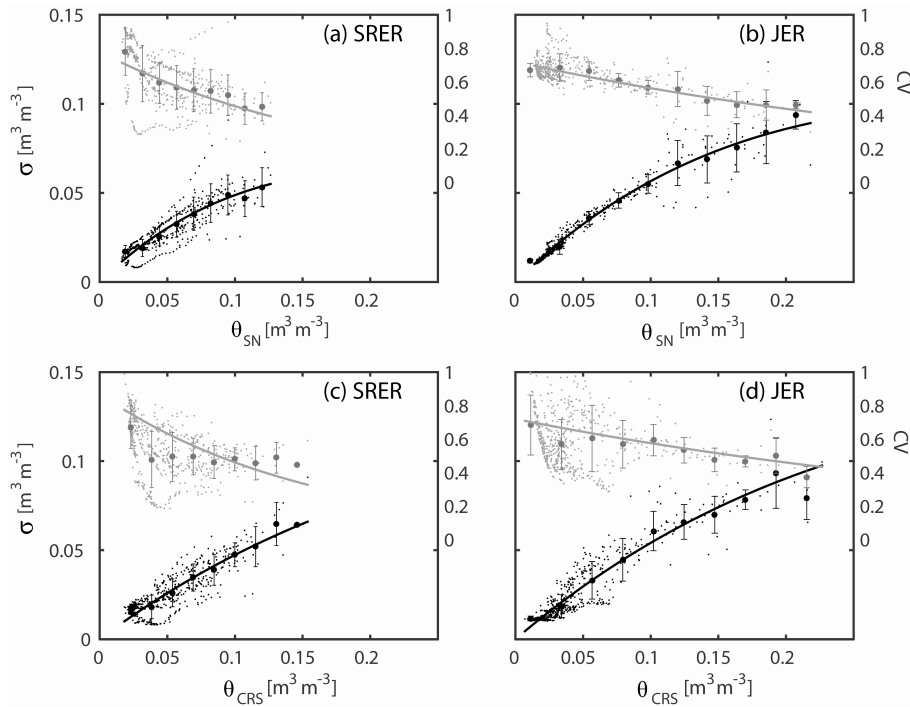
Figure 9. Soil moisture spatial variability as a function of the spatially-averaged distributed sensor network (θ_{SN}, top) and the CRS method (θ_{CRS}, bottom) for **(a, c)** SRER and **(b, d)** JER. Black symbols represent the standard deviation (σ) and gray symbols depict the coefficient of variation (CV). Bin averages and ± 1 standard deviation are shown (circles and error bars) for bin widths of $0.015\,\mathrm{m^3\,m^{-3}}$ at SRER and $0.025\,\mathrm{m^3\,m^{-3}}$ at JER. Regressions for the relations of σ and CV with $<\theta>$ are valid for the entire dataset.

Title Page

Abstract | Introduction

Conclusions | References

Tables | Figures

|◄ | ►|

◄ | ►

Back | Close

Full Screen / Esc

Printer-friendly Version

Interactive Discussion
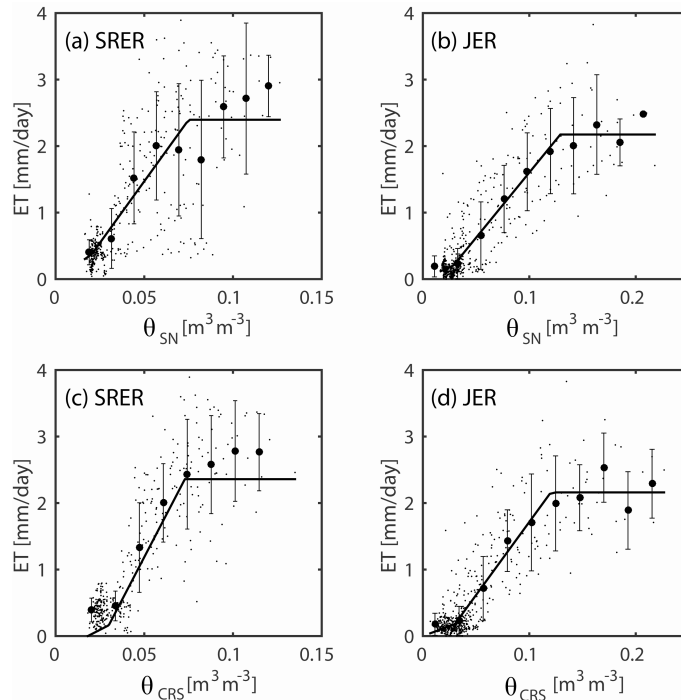
Figure 10. Evapotranspiration relation with the spatially-averaged distributed sensor network (θ_{SN}, top) and the CRS method (θ_{CRS}, bottom) for **(a, c)** SRER and **(b, d)** JER. Bin averages and ± 1 standard deviation are shown (circles and error bars) for bin widths of $0.015\,\mathrm{m^3\,m^{-3}}$ at SRER and $0.025\,\mathrm{m^3\,m^{-3}}$ at JER. Regressions for the relations of ET with $<\theta>$ are valid for the entire dataset.

Title Page

Abstract | Introduction

Conclusions | References

Tables | Figures

|◄ | ►|

◄ | ►

Back | Close

Full Screen / Esc

Printer-friendly Version

Interactive Discussion
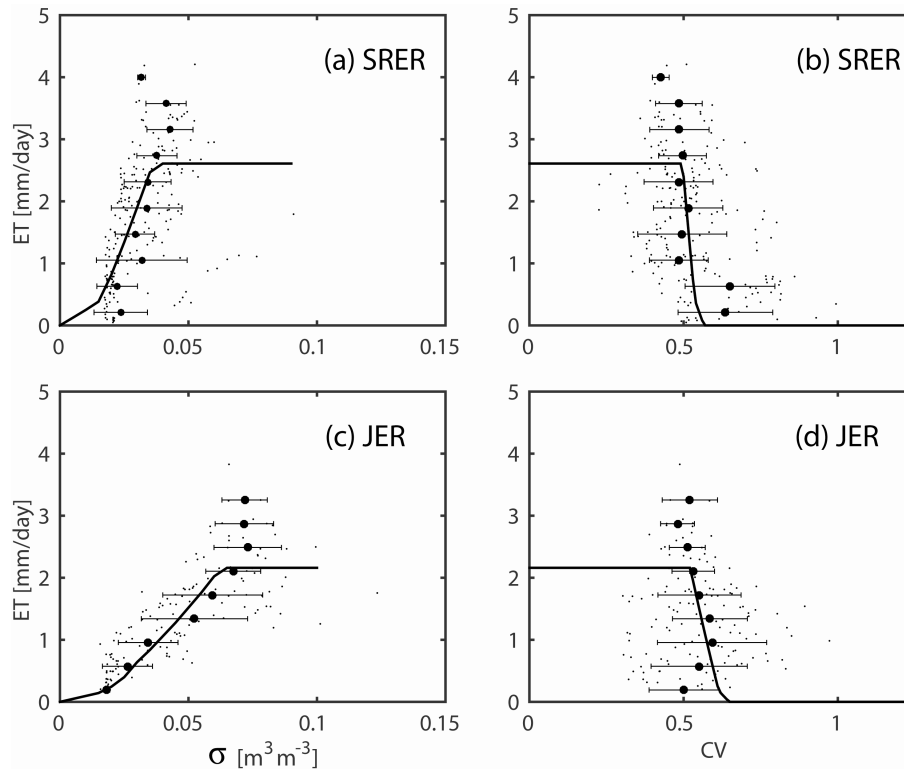
Figure 11. Evapotranspiration relation with the soil moisture standard deviation (σ, left) and the coefficient of variation (CV, right) for **(a, b)** SRER and **(c, d)** JER. Bin averages and ± 1 standard deviation are shown (circles and error bars) for bin widths of $0.33\,\mathrm{mm\,d^{-1}}$. Solid lines represent predicted analytical relationships (not regressions).